Desalination and Water Treatment
www.deswater.com

doi: 10.5004/dwt.2021.27097

221 (2021) 11–22
May

The effects of Ca^{2+} and Mg^{2+} ion concentrations in brine on scaling formation and morphology on metal surfaces

Shengqiang Shen[a,*], Bing Ni[a], Yihao Li[a,b], Xiaohua Liu[a,*]

[a]*Liaoning Key Laboratory of Desalination, School of Energy and Power Engineering, Dalian University of Technology, Dalian 116024, China, emails: zzbshen@dlut.edu.cn (S. Shen), lxh723@dlut.edu.cn (X. Liu), 378459679@qq.com (B. Ni), 364674118@qq.com (Y. Li)*
[b]*Shanghai Marine Diesel Engine Research Institute, Shanghai 200120, China*

Received 4 May 2020; Accepted 21 January 2021

ABSTRACT

The scale formation and morphology for aluminum brass tube surfaces in high-temperature brine were studied and experimented on. The scaling morphology was detected using scanning electron microscopy and an energy-dispersive X-ray spectroscopy. The effects of Ca^{2+} and Mg^{2+} ion concentrations on scaling morphology for $Mg(OH)_2$ crystals and $CaCO_3$ crystals on tube surfaces were investigated. After a piece of metal tube is immersed in high-temperature brine for a period of time, the scaling would appear on the tube surface, primarily composed of $Mg(OH)_2$ crystals and $CaCO_3$ crystals. Scaling structure and crystal morphology are affected by concentrations of Mg^{2+} and Ca^{2+} ions. Appropriate amounts of Mg^{2+} ions could cause $CaCO_3$ crystals to split into scattered irregular crystals on aluminum brass tube surfaces.

Keywords: Scaling; Ion concentration; Brine; Desalination; Crystallization mechanism

1. Introduction

High salinity brine is commonly found in desalination processes, the chemical industry, wastewater treatment plants, food processing, etc. Scale formation is a major problem plaguing high salinity water treatment, especially in evaporation or concentrated heat exchangers. Scaling reduces the heat transfer rate, clogs cross-sectional flow areas, causes corrosion, and even leads to local overheating on heat transfer surfaces. Since it seriously impacts equipment performances and processes, the scaling process garnered much attention. For brine concentrations distilled in heat exchangers, the main factors affecting scaling deposition include temperature, concentration, flow velocity, surface roughness, and free energy. The main scaling contents include $Mg(OH)_2$, $CaCO_3$, and more. It is significant to study the tendency, composition, and morphology of scale in heat exchange equipment for scale prevention, inhibition, and removal.

Alsadaie et al. [1] predicted scale deposition at high temperatures through the dynamic process model of multistage flash evaporation. The results show that the deposition of scale increases with the increase of wall temperature. Pääkkönen et al. [2] indicated that the scaling rate was affected by both wall temperature and flow rate. It was found that the scaling rate decreases with the increase in flow rate at high wall temperatures.

The ion concentration and salinity in brine significantly influenced fouling formation. Peyghambarzadeh et al. [3] analyzed $CaSO_4$ scaling with the Taguchi algorithm. Their results demonstrate that, when compared with flow velocity, temperature, and heat flux, the $CaSO_4$ concentration in solution had a greater effect on scaling rate. Xu et al. [4]

* Corresponding authors.

studied the $CaSO_4$ crystallization process through the static experiment. Results indicated that with a higher concentration of Ca^{2+} ions and SO_4^{2-} ions in the solution, the $CaSO_4$ crystallization rate will increase. Al-Rawajfeh [5] developed the mathematical model for the $CaCO_3$ deposition of seawater with salinity ranging from 2.5% to 6.7%. The results indicated that the deposition rate of $CaCO_3$ increased with an increase in salinity. Liu [6] studied the seawater scaling process during falling film evaporation outside the horizontal tubes. The salinity for the experimental seawater ranged from 3.5% to 7%. The results concluded that the deposition rate of scale increased with increased salinity.

The surface properties also have some influence on fouling formation. Kazi et al. [7] posited that the scale deposition amount increased with surface energy, and scaling preferred to adhere to metal surfaces with high surface energy. However, Zettler et al. [8] displayed that surface energy alone was not sufficient to describe scale deposition characteristics. Stärk et al. [9] studied the effects of different metal tubes on scale deposition characteristics. The results indicated that on metal tube surfaces with higher surface energy, the quality of Mg content in the scale per unit area was higher, but the deposition amount of the scale was smaller. Therefore, the scale deposition characteristics were not simply related due to surface energy. Magnesium salts formations on metal surfaces will affect $CaCO_3$ crystal precipitation. Therefore, the interaction between $Mg(OH)_2$ crystal and $CaCO_3$ crystal should be considered in any study of scale deposition characteristics.

Some studies have also investigated scaling layers. Wildebrand et al. [10] studied scale formation from artificial seawater on horizontal tubes in a multiple-effect evaporator. The salinity ranged from 3.5% to 6.5%. The results indicated that $Mg(OH)_2$ crystals could more easily deposit on metal surfaces and concluded that $Mg(OH)_2$ crystals formation occurs prior to $CaCO_3$ crystals, and $CaCO_3$ crystals would prevent $Mg(OH)_2$ crystals from forming. Krömer et al. [11] and Stärk et al. [12] investigated scale formation in a multiple-effect evaporator. The salinity was 4.5%~6.5%. By using scanning electron microscopy (SEM) and X-ray diffraction (XRD) to analyze scaling, they found that the $CaCO_3$ crystals formed on top of $Mg(OH)_2$ crystals, and when Mg^{2+} ion concentration decreased, $CaCO_3$ deposits increased.

The crystals exhibited different morphologies under different conditions. $Mg(OH)_2$ crystals exhibited a triangular conical structure in a saturated solution of $Mg(OH)_2$ with NaCl. $Mg(OH)_2$ crystals forming in the seawater exhibiting a flaky structure with different degrees of agglomeration [13–16]. Due to different nucleation methods, $CaCO_3$ crystals can be divided into three forms, aragonite, calcite, and vaterite. Calcite is a hard scale, which is the most stable and difficult to remove. Vaterite is a soft scale and easy to remove. The hardness and removal difficulty for aragonite are both moderate. Mg^{2+} ion concentration inhibits nucleation of calcite in $CaCO_3$ crystals, leading to a transition from calcite to aragonite [17]. However, different morphologies inherent in $CaCO_3$ crystals would transform into stable calcite $CaCO_3$ crystals after a long period of time.

Liu et al. [18] and Zhang and Dawe [19] studied the effects of Mg^{2+} ions on $CaCO_3$ precipitation in a saturated $CaCO_3$ solution. Liu et al. [18] concluded that when the Mg^{2+} ion concentration exceeded 0.50 mmol L^{-1}, the Mg^{2+} ions exhibited a strong inhibitory effect on $CaCO_3$ crystals. Zhang and Dawe [19] believed that the presence of Mg^{2+} ions would reduce the calcite growth rate. A solution with a higher concentration ratio of Mg^{2+} ions to Ca^{2+} ions greatly slowed the growth rate of $CaCO_3$ crystals. Yang et al. [20] explored the effects of Mg^{2+} ions on $CaCO_3$ scale formation on metal surfaces in hard water. It was discovered that Mg^{2+} ions could obviously inhibit $CaCO_3$ crystal growth.

As mentioned above, many studies focus on scale formation and its content. Studies on the interactions between different ions during scale formation are insufficient. Some literature reported the effects of Mg^{2+} ions on $CaCO_3$ crystal formation. The effects of Ca^{2+} ions on $Mg(OH)_2$ crystal formation have rarely been reported. Furthermore, research on the morphologies and transformations of scales while interacting with calcium and magnesium ions at different concentrations is also lacking.

Understanding the influence of ion concentrations in brine on the scaling morphology is crucial for revealing the mechanisms driving scale formation. Scales with different crystal morphologies on metal surfaces require different prevention and removal measures; therefore, it is also critical for the blueprints for and operations of desalination plants and high salinity water treatment plants to reveal the compositions and morphologies of scales. It will help establish a suitable pretreatment method to prevent heat exchangers from scaling and select suitable scale removal methods to remove them on heat transfer surfaces. In this paper, we will focus on the effects of Ca^{2+} and Mg^{2+} ion concentrations on crystal scale morphologies. This paper will focus on the effects of Ca^{2+} and Mg^{2+} ion concentrations on scale formations and crystal morphologies of scaling.

2. Experimental testing method

According to natural seawater composition and the proportions of each composition, the brine is configured by dissolving a certain molar concentration ratio of NaCl, $NaSO_4$, $CaCl_2$, $MgSO_4$, $MgCl_2$, and $NaHCO_3$ salts into deionized water. Table 1 gives the ion concentrations in normal brine. Brine salinity is 10%. Titanium and aluminum brass tubes were used in the experiment. The two metals have excellent corrosion resistance in seawater and are commonly used as heat exchange tube materials in seawater desalination and high salt wastewater treatment devices. The element compositions for the metal tube materials are shown in Table 2.

Table 1
Ion concentrations in brine at a salinity of 10% (mol L^{-1})

Salinity	10%
Mg^{2+}	0.154
Ca^{2+}	0.032
SO_4^{2-}	0.081
HCO_3^-	0.0071
Cl^-	1.610
Na^+	1.407

To analyze how Ca^{2+} and Mg^{2+} ion concentrations influence on the morphologies of $CaCO_3$ crystals and $Mg(OH)_2$ crystals, five groups of brine with different Ca^{2+} ion concentrations and five groups of brine with different Mg^{2+} ion concentrations were prepared. In the brine, the other ion concentrations were kept constant, as shown in Table 1. The concentrations of the Ca^{2+} ions in brine were increased equivalently from 0 to 0.032 mol L^{-1} as shown in Table 3. The concentrations of the Mg^{2+} ions in brine were increased equivalently from 0 to 0.154 mol L^{-1} as shown in Table 4. The salinity of the prepared brine changed slightly, but the effects of Ca^{2+} and Mg^{2+} ions on the morphologies of scaling crystals were primarily studied in the brine experiment, and the influences of salinity differences on the experiment results could be ignored.

Figs. 1 and 2 depict diagrams and pictures of the brine scaling test benchmarks, and the main equipment models and parameters are shown in Table 5. Several beakers were put on the beaker. Brine was placed in the beakers, and a section of metal tube was immersed in the brine. In experiments, the brine temperature was maintained at 80°C. When the metal tube was immersed in high-temperature brine for 60 h, and then the metal tubes were removed from the beaker. Visible to the naked eye, scaling was clearly visible on the metal tube surface. The de-ionized water was used to dissolve the soluble salt adhering to the metal tube surface. Through detection and analysis, it was found that when XRD had determined the type of mixed substance, the peak values for different crystals would overlap, which caused issues distinguishing between crystal types. Therefore, SEM and energy-dispersive X-ray spectroscopy (EDX) were used to detect scaling. The results (crystal morphologies and types of scaling) were compared with published literature.

3. Results and discussion

3.1. Effects of metal types on scaling formation and discussions

In this experiment, brine with 10% salinity was selected as the solution, and titanium and aluminum brass tubes were selected as the experimental tubes. The ion concentrations are shown in Table 1.

The SEM images for scaling on titanium and aluminum brass tube surfaces are presented in Fig. 3. The EDX analyzed the results from scaling at rectangular regions marked, 1, 2, 3, and 4 in Fig. 3 respectively, as shown in Fig. 4 and Table 6.

According to the crystal morphology of scaling shown in Fig. 3 and the composition and content of each element given in Fig. 4 and Table 6, the scaling on the two kinds of metal tubes is primarily composed of $Mg(OH)_2$ and $CaCO_3$. $CaCO_3$ crystals and $Mg(OH)_2$ crystals exhibit different morphologies on titanium and aluminum brass tubes. $CaCO_3$ and $Mg(OH)_2$ have reverse solubility. When brine temperature is 80°C and the salinity is 10%, the $CaCO_3$ and $Mg(OH)_2$ in the solution have reached supersaturation, and the scale-forming ions crystallize and precipitate onto the metal tube surface to form scaling [21]. Compared with rectangular regions 1 and 3 in Fig. 3, it can be seen that the $Mg(OH)_2$ crystal size is smaller than that of the $CaCO_3$ crystal. The scaling on titanium tubes includes horizontal flaky $Mg(OH)_2$ crystals and octahedral $CaCO_3$ crystals, while the scaling on aluminum brass tubes includes vertical flaky $Mg(OH)_2$ crystals, octahedral $CaCO_3$ crystals, and irregular $CaCO_3$ crystals. The vertical flake $Mg(OH)_2$ crystals are agglomerated on the aluminum brass tube and are honeycomb-shaped.

In addition, more $CaCO_3$ and $Mg(OH)_2$ crystals formed on the aluminum brass tube than on the titanium ones. The differences in scaling amount on different tubes reflect the relationships between scaling deposition and metal surface characteristics. The surface energy for the aluminum brass tube is higher than that of the titanium tube, and $CaCO_3$ and $Mg(OH)_2$ crystals deposit more easily on metal surfaces with high surface energy, so the amount of scale deposition on aluminum brass tubes is larger than that on titanium tubes.

Table 3
Ca^{2+} ion concentration (mol L^{-1})

Groups	Ca^{2+}
1	0
2	0.008
3	0.016
4	0.024
5	0.032

Table 4
Mg^{2+} ion concentration (mol L^{-1})

Groups	Mg^{2+}
6	0
7	0.038
8	0.077
9	0.115
10	0.154

Table 2
Element compositions of metal tubes

Metal	Major elements						Other elements	
Ti(TA2)	Ti	C	H	Fe	O	N	Single	Sum
	98.735	0.10	0.015	0.30	0.30	0.05	0.1	0.4
Cu(HAl77-2)	Cu	Al	Fe	Pb	As	Zn	Mn/Ni/Si	
	79	2	0.06	0.07	0.05	Margin	<0.1	

It can be concluded from the composition of brine scaling that the presence of Ca^{2+} ions and Mg^{2+} ions in brine is the main cause behind brine scaling, which is also the reason why people often add decalcium and demagnesium in brine pretreatment to prevent heat exchanger scaling. What is the effect of Ca^{2+} ion and Mg^{2+} ion content in brine on scale formation? To clarify the effects of Ca^{2+} ion and Mg^{2+} ion concentrations on forming $CaCO_3$ and $Mg(OH)_2$ crystals, the following study of scaling morphology on the surface of aluminum brass tubes are conducted under different Ca^{2+} and Mg^{2+} ion concentrations.

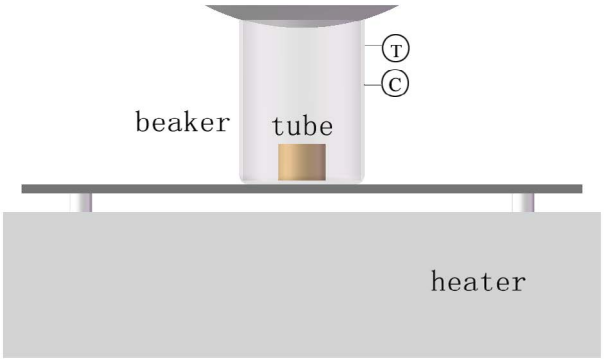

Fig. 1. Brine scaling test bench diagram.

Fig. 2. Brine scaling test bench picture.

3.2. Effects of ion concentrations on scaling formation and discussions

3.2.1. Effects of Ca^{2+} ion concentrations on scale crystal morphologies

To analyze how the Ca^{2+} ion concentrations influence $CaCO_3$ crystal and $Mg(OH)_2$ crystal morphologies, five groups of brine with different Ca^{2+} ion concentrations were selected for the following experiments. The concentrations of Ca^{2+} ion are shown in Table 3.

3.2.1.1. Brine without Ca^{2+}

The experiment was conducted using brine without Ca^{2+} ion. The experimental procedure is the same as the previous one. The SEM image for scaling on aluminum brass tubes with 10,000× magnification is displayed in Fig. 5. The element analysis results for EDX scaling at regions 1 and 2 marked in Fig. 5 are shown in Fig. 6 and Table 7.

When the brine does not contain Ca^{2+}, a large number of triangular cone crystals are deposited on the aluminum brass tube surface, as shown in the rectangular region 1

Table 5
Main equipment

Name	Model	Parameter
Heater	ZB3020JR	0~400°C
Beaker	–	0~200 mL
Scanning electron microscopy	QUANTA	0–40,000 times

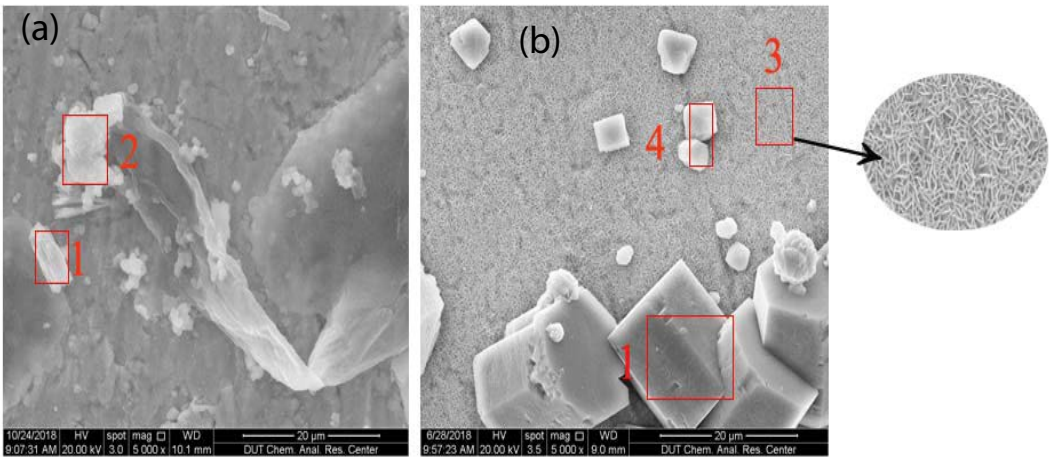

Fig. 3. SEM images of scaling on titanium and aluminum brass tubes. Mag 5,000× on (a) Ti tube and (b) brass tube [(1) $CaCO_3$ (octahedron), (2) $Mg(OH)_2$ (horizontal flakes), (3) $Mg(OH)_2$ (honeycomb), and (4) $CaCO_3$ (irregularity)].

Table 6
Components of local scaling (%)

	a	*b*	*c*	*d*
Element	Mass fraction	Mass fraction	Mass fraction	Mass fraction
O	19.13	57.45	47.34	35.06
Mg	0.41	16.39	9.62	4.42
Si	0.36	10.86	7.42	2.66
Cl	0.17	2.05	0.90	4.81
Ca	18.11	0.44	0.61	1.29
C	46.88	–	16.42	17.40
Ti	13.91	9.31	–	–
Na	0.5	1.25	–	–
Cu	–	–	12.82	25.70
Zn	–	–	3.2	6.18
Others	0.52	2.24	1.67	2.48
Total	100.00	100.00	100.00	100.00

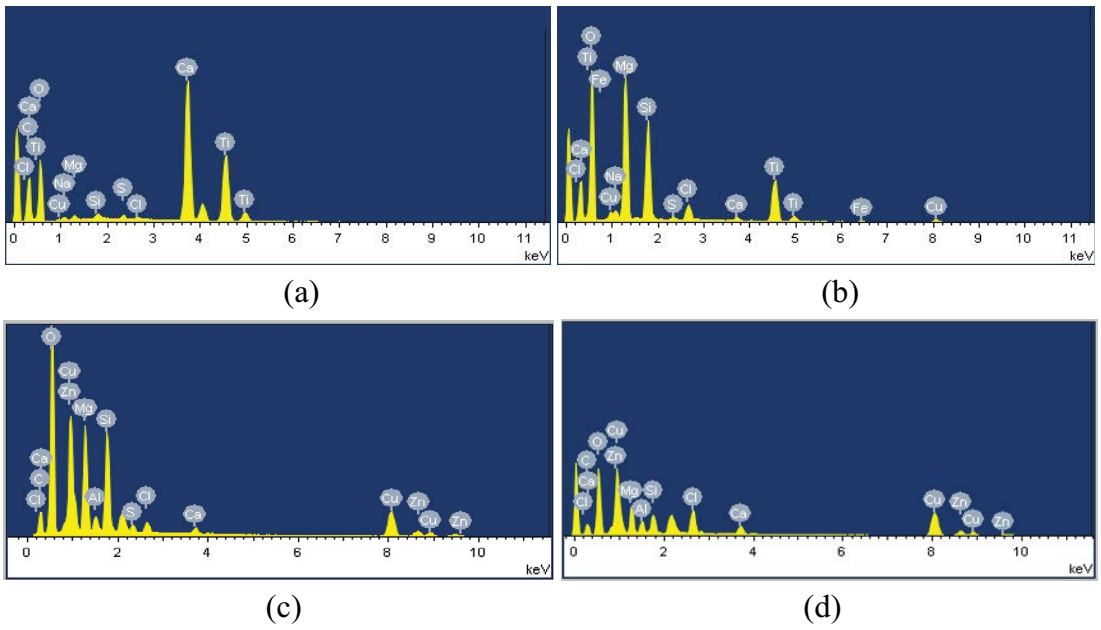

Fig. 4. EDX results of local scaling region: (a) region 1, (b) region 2, (c) region 3, and (d) region 4.

marked in Fig. 5. In some areas, large flaky crystals could be observed on the aluminum brass tube surface, as shown at rectangular region 2 marked in Fig. 5. According to the crystal morphologies in Fig. 5, and the composition data in Fig. 6 and Table 7, it is clear that the triangular conical crystals are $Mg(OH)_2$, and the large flaky crystals are magnesium, oxygen-containing scale.

The brine contains a large amount of Na^+ ions. The radius of Na^+ ions is similar to that of the Mg^{2+} ions. Therefore, while forming $Mg(OH)_2$ crystals, some Na^+ ions would easily replace some Mg^{2+} ions in $Mg(OH)_6^{4-}$ (the basic unit that forms $Mg(OH)_2$), which would reduce the energy needed for growing $Mg(OH)_2$ crystals. Therefore, the growth rate for $Mg(OH)_2$ crystals changes in different directions [13], and its crystals present a triangular cone morphology.

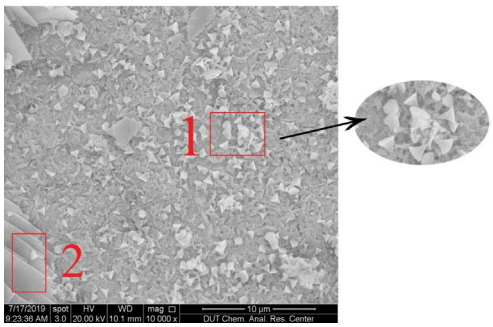

Fig. 5. SEM image of scaling with zero Ca^{2+} ion brine. Mag 10,000× (on Cu tube) [(1) $Mg(OH)_2$ (triangular cone) and (2) Mg, O-containing scale (flake)].

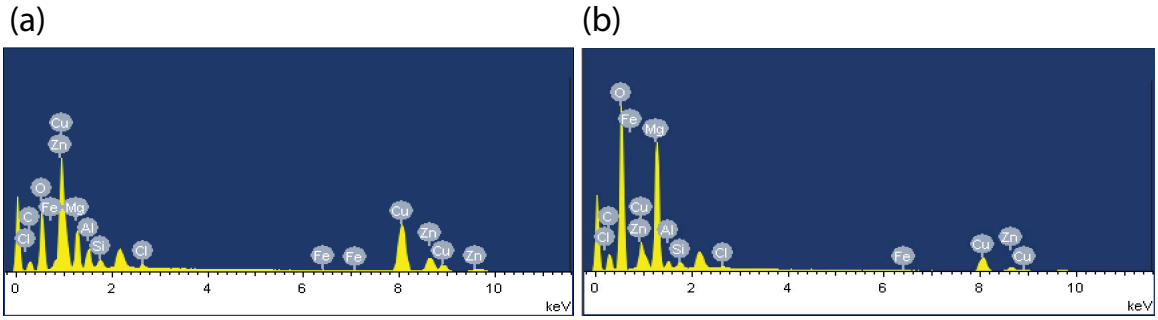

Fig. 6. EDX results for local scaling with zero Ca^{2+} ion: (a) region 1 and (b) region 2.

Because no Ca^{2+} ions are in the brine, the scale composition is only $Mg(OH)_2$ crystals. These results can also be used as a reference for the effects of Ca^{2+} ions on compositions of scale.

3.2.1.2. Brine with Ca^{2+} ion concentration of 0.008 mol L^{-1}

When the Ca^{2+} ion concentration is 0.008 mol L^{-1}, the concentration ratio of Mg^{2+} ions and Ca^{2+} ions is 19.31. With this brine, SEM morphology images of scaling on the aluminum brass tube surface at different locations are shown in Fig. 7. In this case, both $CaCO_3$ and $Mg(OH)_2$ were found in the scaling. The $CaCO_3$ crystal was octahedral with some cracking, as shown in Fig. 7. $Mg(OH)_2$ crystals presented both horizontal and vertical flakes, as shown in Fig. 7b.

Table 7
Components of local scaling with zero Ca^{2+} ion (%)

Element	*a*	*b*
	Mass fraction	Mass fraction
C	14.64	15.98
O	31.03	49.21
Mg	14.58	17.57
Fe	0.37	0.37
Cu	26.60	11.13
Zn	9.10	3.87
Others	1.98	1.31
Totals	100.00	100.00

Comparing Figs. 5 and 7, with Ca^{2+} ion concentration increasing from 0 to 0.008 mol L^{-1}, the $Mg(OH)_2$ crystals transform from triangular cones to flaky ones at the same Na^+ ion concentration. When the external physical and chemical conditions are different, different crystal structures can be formed for substances with the same chemical compositions. Since Ca^{2+} ion was present, the polar $CaCO_3$ crystal formed. It affected the growth rate of $Mg(OH)_2$ in different directions and weakened the effects of Na^+ ion on $Mg(OH)_2$ crystal development. Therefore, $Mg(OH)_2$ crystals no longer consisted of a triangular cone morphology.

3.2.1.3. Brine with Ca^{2+} ion concentration of 0.016 mol L^{-1}

When the Ca^{2+} ion concentration is 0.016 mol L^{-1} and the concentration ratio for Mg^{2+} ions and Ca^{2+} ions is 9.65, SEM morphology images of surface scaling on the aluminum brass tube at different locations are shown in Fig. 8.

In this case, $Mg(OH)_2$ crystals presented a honeycomb morphology on the aluminum brass tube with no

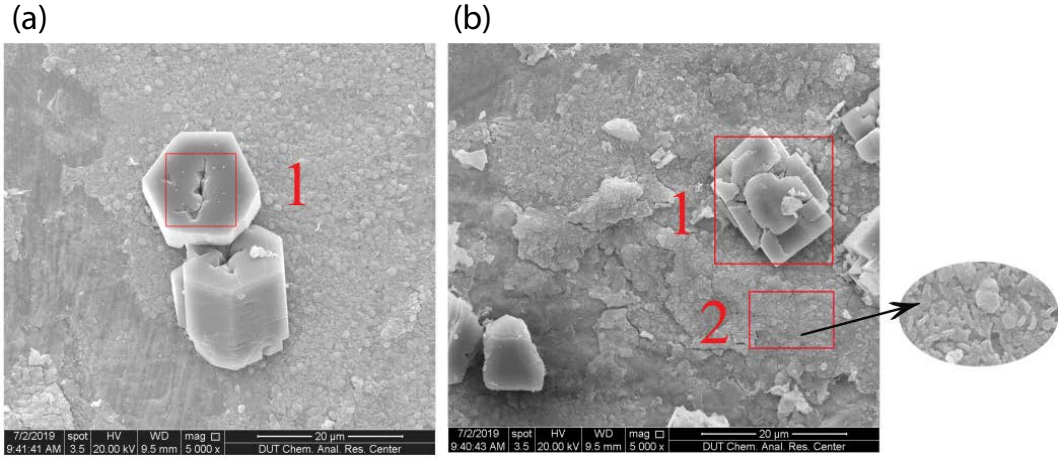

Fig. 7. SEM images of scaling with Ca^{2+} ion concentration of 0.008 mol L^{-1}: (a and b) Mag 5,000× [(1) $CaCO_3$ (octahedron) and (2) $Mg(OH)_2$ (flake)].

horizontal flaky crystal, as shown in Fig. 8b. $CaCO_3$ was a polar crystal. When $CaCO_3$ crystal adhered to the surface of the aluminum brass tube, under external polarity force, polar $Mg(OH)_2$ crystal produced dislocations, causing slippage during formation. Compared with Figs. 7 and 8, with an increase in Ca^{2+} ion concentration, the deposition amount for $CaCO_3$ crystal increased, and the force of $CaCO_3$ crystals on $Mg(OH)_2$ crystal gradually increased, which caused $Mg(OH)_2$ crystals to change from flaked to agglomerate. Compared with $CaCO_3$ crystals in Fig. 7a, the cracks inside $CaCO_3$ crystals became bigger in Fig. 8a. Some of the $CaCO_3$ crystals cracked, and the original octahedral morphology became small irregular crystals, as shown in Fig. 8b.

3.2.1.4. Brine with Ca^{2+} ion concentration of 0.024 mol L^{-1}

When the Ca^{2+} ion concentration is 0.024 mol L^{-1} and the concentration ratio of Mg^{2+} ion and Ca^{2+} ion is 6.44, SEM morphology image of surface scaling on the aluminum brass tube is shown in Fig. 9.

The scaling on the aluminum brass tube included octahedral $CaCO_3$ crystals, irregular $CaCO_3$ crystals, and honeycomb $Mg(OH)_2$ crystals, as shown in Fig. 9. $Mg(OH)_2$ crystals on the base layer were still a honeycomb aggregation, as shown in Fig. 9. Compared with Fig. 8, scattered irregular $CaCO_3$ crystals appeared in Fig. 9, and irregular crystals contained both calcium and magnesium elements as shown in Fig. 4 and Table 6. The irregular crystals sizes in the surface layer were minor, and the element composition of the base layer could be detected by EDX when detecting element compositions of irregular crystals. Therefore, the crystals might not contain a magnesium element or contain less, and the main element of the crystals was calcium. It would be reasonable to consider that these small crystals were irregular $CaCO_3$ crystals.

The crystal structure could be changed by substituting particles (isomorphism), and replacing partial particles is called an incomplete isomorphism. According to the empirical data for atom substitution, it is known that the radius r_1 of Ca^{2+} ions is 0.1 nm and the radius r of Mg^{2+} ions is 0.072 nm, $(r_1 - r)/r_1 \in 25\%\sim40\%$, which could only form a finite substitution. The percentage of Mg^{2+} ions that replaced Ca^{2+} ions in calcite reached 22% [22], and the higher Mg^{2+} ion concentration in solution would make it easier to replace Ca^{2+} ions in the lattice. Throughout the experiment, Ca^{2+} ions would be continuously captured during $CaCO_3$ crystal formation, but due to crystal defects, some Mg^{2+} ions would take the places of Ca^{2+} ions. Internal stress was present in the crystals containing Mg^{2+} ions, which is in an unstable state and led to the $CaCO_3$ crystals cracking and finally splitting into small irregular crystals as shown in Figs. 7~9.

3.2.2. Effects of Mg^{2+} ion concentrations on the scale crystal morphologies

In the section above, the effects of Ca^{2+} ion concentrations on scaling formation were analyzed. To analyze how Mg^{2+} ion concentrations impact on $CaCO_3$ crystal and $Mg(OH)_2$ crystal morphologies, five groups of brine with different Mg^{2+} ion concentrations were selected for the following experiments. The concentration of Mg^{2+} ions is shown in Table 4.

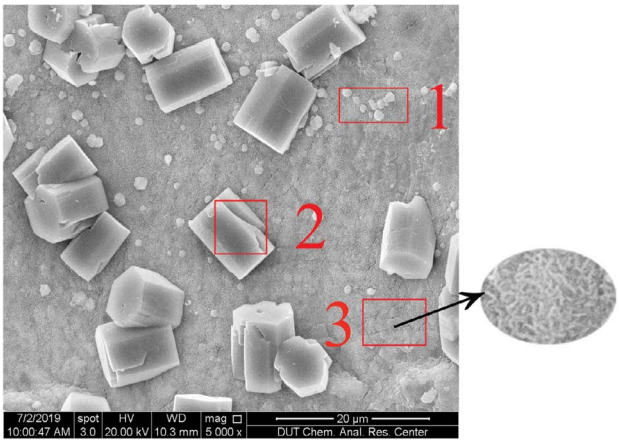

Fig. 9. SEM image of scaling with Ca^{2+} ion concentration of 0.024 mol L^{-1}: Mag 5,000× [(1) $CaCO_3$ (irregularity), (2) $CaCO_3$ (octahedron), and (3) $Mg(OH)_2$ (honeycomb)].

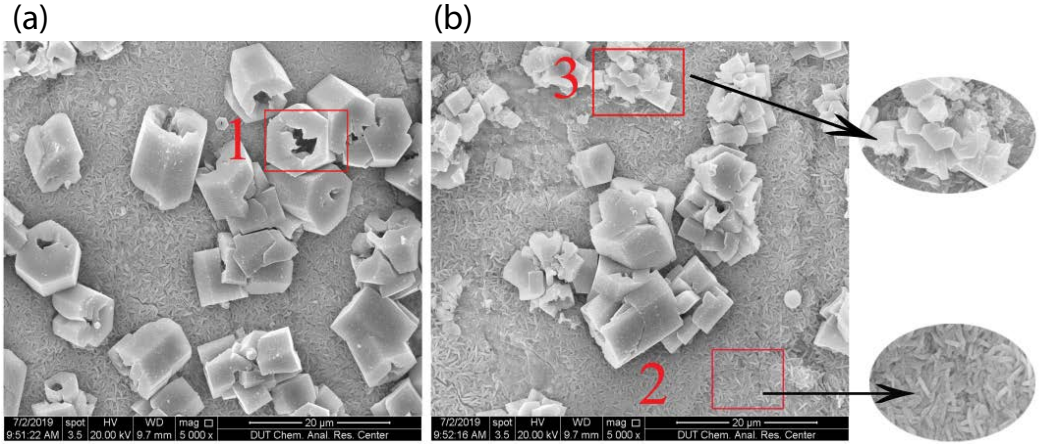

Fig. 8. SEM images of scaling with Ca^{2+} ion concentration of 0.016 mol L^{-1}: (a and b) Mag 5,000× [(1) $CaCO_3$ (octahedron), (2) $Mg(OH)_2$ (honeycomb), and (3) $CaCO_3$ (irregularity)].

3.2.2.1. Brine without Mg^{2+}

Brine without Mg^{2+} ion is selected for the scaling experiment. The experimental procedure is the same as the previous one. The SEM morphologies of the surface scaling on the aluminum brass tube are shown in Fig. 10. The EDX results from scaling at the 1, 2, and 3 rectangular regions marked in Fig. 10 are shown in Fig. 11 and Table 8.

It could be predicted that $Mg(OH)_2$ was not detected in surface scaling on the tube due to the absence of Mg^{2+} in the brine. According to the crystal morphology in Fig. 10 and composition data in Fig. 11 and Table 8, the main component for scaling is $CaCO_3$. The main part of the scale presented complex and overlapped plate-like crystals, and others included hexahedral crystals and needle-like crystals. The complex overlapped plate-like structures of $CaCO_3$ crystals were formed due to the presence of NaCl in the solution [23].

3.2.2.2. Brine with Mg^{2+} ion concentration of 0.038 mol L^{-1}

When the Mg^{2+} ion concentration is 0.038 mol L^{-1} and the concentration ratio of Mg^{2+} and Ca^{2+} ions is 1.21, the SEM morphology image of surface scaling on the aluminum brass tube is shown in Fig. 12. Scaling on the aluminum brass tube included octahedral $CaCO_3$ crystals, irregular $CaCO_3$ crystals, overlapped plate-like $CaCO_3$ crystals, and honeycomb $Mg(OH)_2$ crystals.

When the Mg^{2+} ion concentration increased from 0 to 0.038 mol L^{-1}, $Mg(OH)_2$ crystals precipitated, which changed the growth rate of $CaCO_3$ crystals in different directions. $CaCO_3$ crystals changed from overlapping

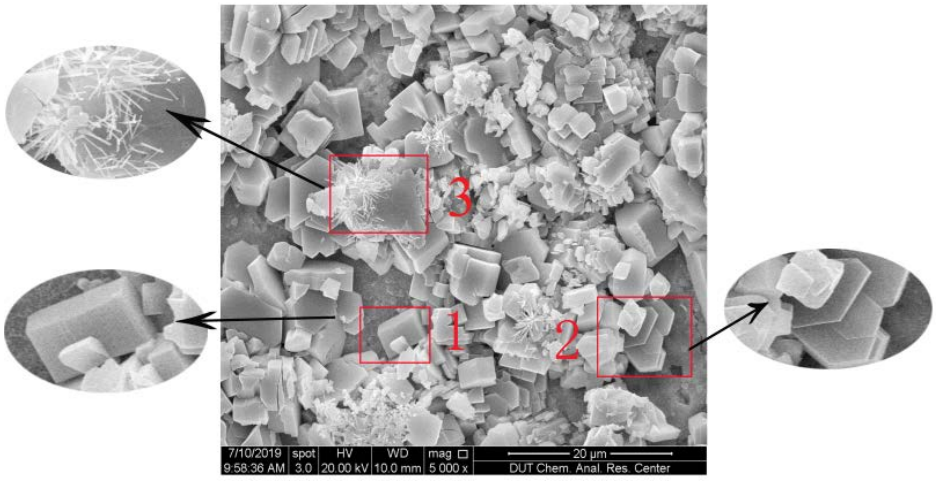

Fig. 10. SEM image of scaling without Mg^{2+}: Mag 5,000× [(1) $CaCO_3$ (hexahedron), (2) $CaCO_3$ (overlapping plates), (3) $CaCO_3$ (needle)].

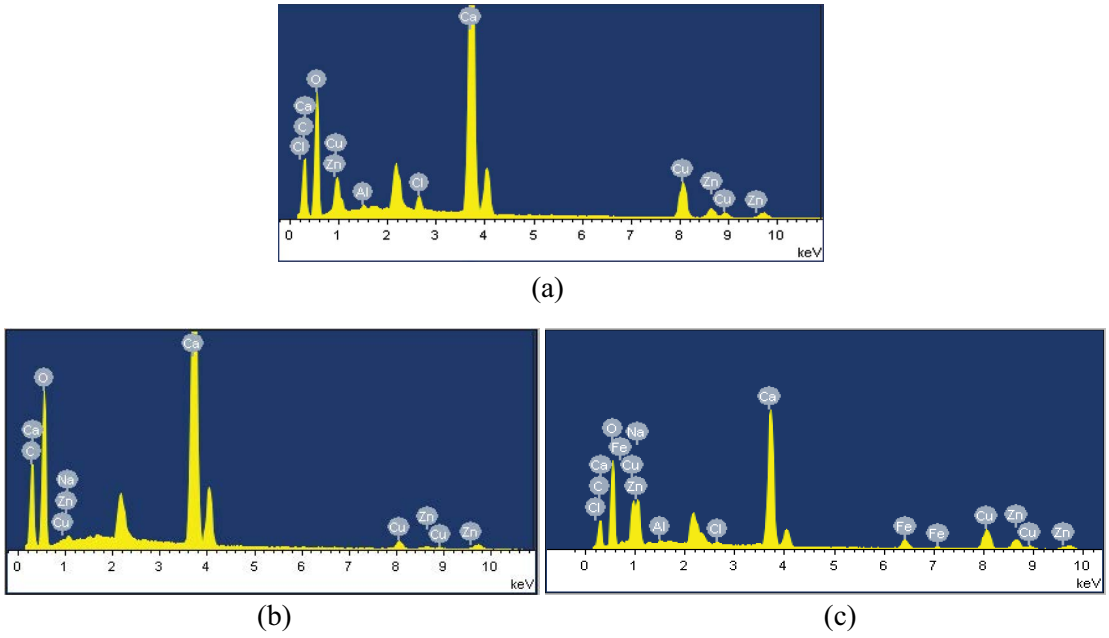

Fig. 11. EDX results of local scaling regions without Mg^{2+} ions: (a) region 1, (b) region 2, and (c) region 3.

Table 8
Components of local scaling with zero Mg^{2+} ion (%)

Element	*a*	*b*	*c*
	Mass fraction	Mass fraction	Mass fraction
C	17.51	15.70	16.94
O	39.07	49.60	38.51
Ca	25.60	30.67	16.80
Cu	12.74	2.79	12.50
Zn	4.06	0.73	7.76
Na	–	0.50	4.30
Fe	–	–	2.57
Others	1.02	–	0.61
Total	100.00	100.00	100.00

plate-like crystals to octahedral crystals, and some octahedral $CaCO_3$ crystals cracked due to lattice distortion when the Mg^{2+} ion concentration is 0.038 mol L^{-1}. Comparing the rectangular regions 1 and 4 in Fig. 12, it could be seen that the sizes of the overlapping plate-like $CaCO_3$ crystals were smaller than that of the octahedral $CaCO_3$ crystals, therefore, when the $CaCO_3$ crystal changed from the overlapping plate-like to the octahedral morphology, it is not conducive to the removing scaling.

3.2.2.3. Brine with Mg^{2+} ion concentration of 0.077 mol L^{-1}

With the Mg^{2+} ion concentration at 0.077 mol L^{-1} and the concentration ratio of Mg^{2+} ions and Ca^{2+} ions at 2.41, the SEM morphology image of surface scaling on the aluminum brass tube is shown in Fig. 13. Scaling on the aluminum brass tube included octahedral $CaCO_3$ crystals, irregular $CaCO_3$ crystals, and honeycomb $Mg(OH)_2$ crystals, as shown in Fig. 13.

When the Mg^{2+} ion concentration in the brine increased to 0.077 mol L^{-1}, scattered and irregular $CaCO_3$ crystals began to appear after octahedral $CaCO_3$ crystals crack. Under these conditions, $Mg(OH)_2$ crystals would remain a morphology of agglomeration and not affected by increases in Mg^{2+} ions.

3.2.2.4. Brine with Mg^{2+} ion concentration of 0.115 mol L^{-1}.

When the Mg^{2+} ion concentration is 0.115 mol L^{-1} and the concentration ratio of Mg^{2+} ions and Ca^{2+} ions is 3.62, the SEM morphology of surface scaling on the aluminum brass tube is shown in Fig. 14. The image shows that the scaling on the aluminum brass tube included octahedral $CaCO_3$ crystals, irregular $CaCO_3$ crystals, and honeycomb $Mg(OH)_2$ crystals. It also shows that no significant changes occurred in the crystal morphologies for Mg^{2+} ion concentration from 0.077 to 0.115 mol L^{-1}

Compared with Fig. 3, when the Mg^{2+} ion concentration is increased to 0.154 mol L^{-1}, crystal morphologies on the aluminum brass tube exhibited no obvious change with the aforementioned results.

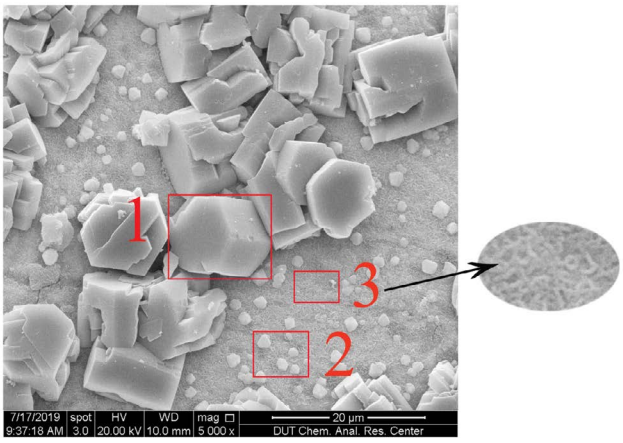

Fig. 13. SEM image of scaling with Mg^{2+} ion concentration of 0.077 mol L^{-1}: Mag 5,000× [(1) $CaCO_3$ (octahedron), (2) $CaCO_3$ (irregularity), and (3) $Mg(OH)_2$ (honeycomb)].

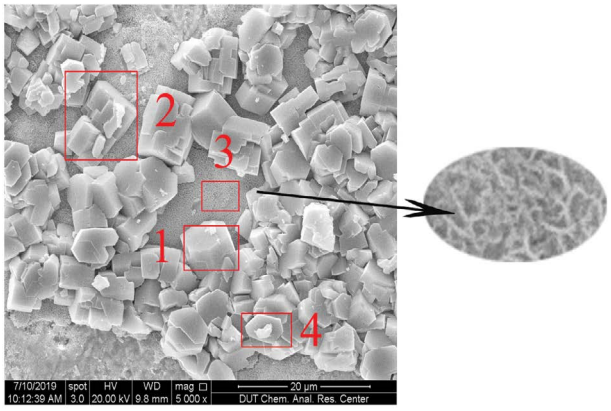

Fig. 12. SEM image of scaling with Mg^{2+} ion concentration of 0.038 mol L^{-1}: Mag 5,000× (on Cu tube) [(1) $CaCO_3$ (octahedron), (2) $CaCO_3$ (irregularity), (3) $Mg(OH)_2$ (honeycomb), and (4) $CaCO_3$ (overlapping plates)].

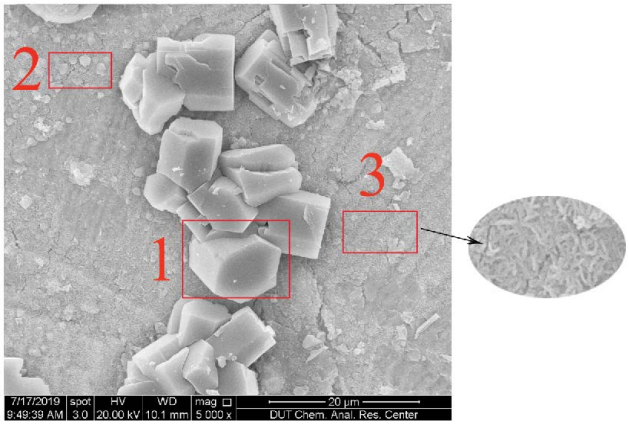

Fig. 14. SEM image of scaling with Mg^{2+} ion concentration of 0.115 mol L^{-1}: Mag 5,000× [(1) $CaCO_3$ (octahedron), (2) $CaCO_3$ (irregularity), and (3) $Mg(OH)_2$ (honeycomb)].

The morphologies for $CaCO_3$ crystals at different concentration ratios for Ca^{2+} to Mg^{2+} ions are summarized in Fig. 15. For the brine with high Ca^{2+} ion concentrations, with the increase in Mg^{2+} ion concentration, the $CaCO_3$ crystal morphologies transformed from overlapping plate-like to octahedral, and some of the octahedral crystals cracked to form scattered irregular crystals, as pictures 6, 7, 8, 9, and 10 shown in Fig. 15. For the brine with a high Mg^{2+} ion concentration, with the increase in Ca^{2+} ion concentration, octahedral $CaCO_3$ crystal cracked, and split into scattered irregular crystals, as pictures 2, 3, 4, and 5 shown in Fig. 15.

The morphologies of $Mg(OH)_2$ crystals at different concentration ratios of Ca^{2+} to Mg^{2+} ions are summarized in

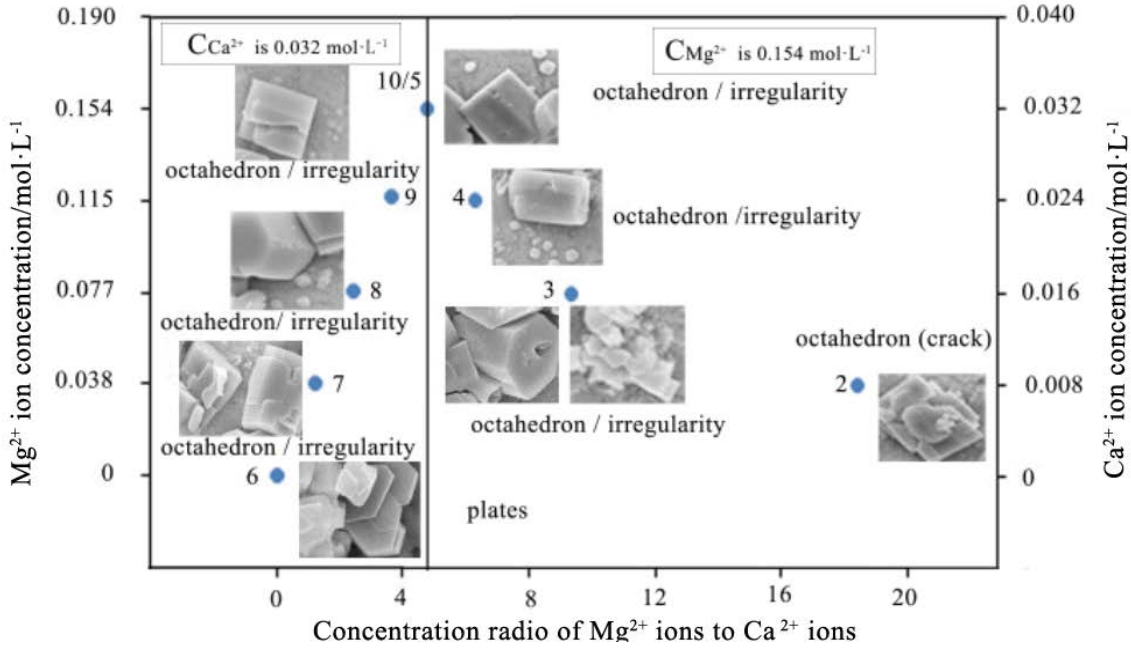

Fig. 15. Changes in the morphologies of $CaCO_3$ crystals at different concentration ratios.

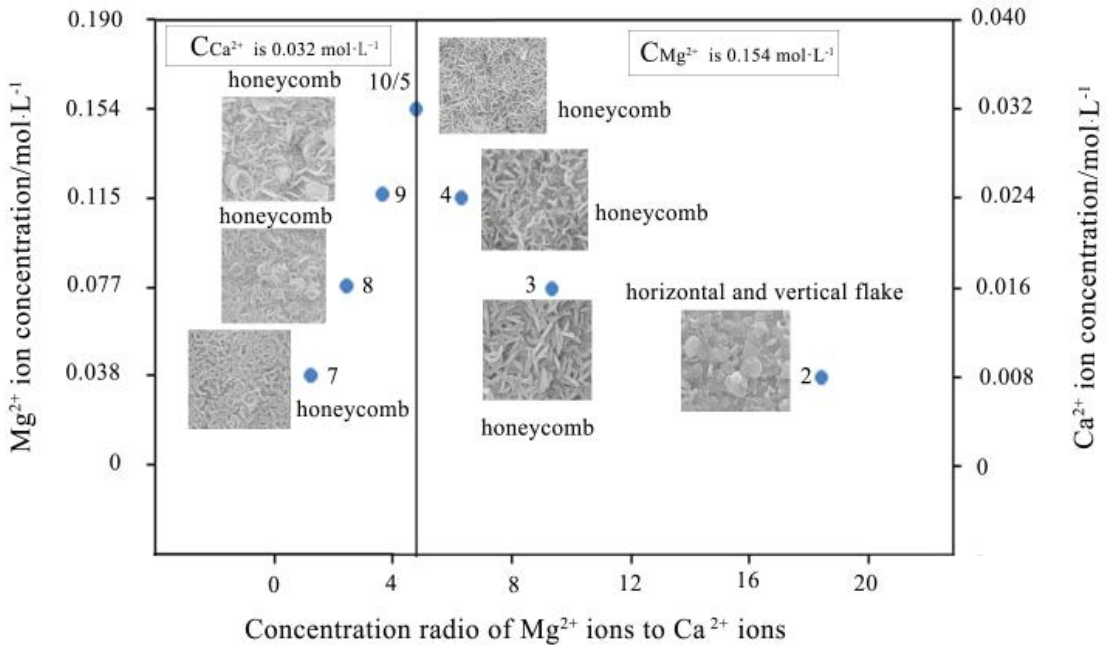

Fig. 16. Changes in the morphologies of $Mg(OH)_2$ crystals at different concentration ratios.

Fig. 16. For the brine with a high Mg^{2+} ion concentration, with an increase in Ca^{2+} ion concentration, the $Mg(OH)_2$ crystal morphology transformed from flake to agglomerated morphology, as pictures 2, 3, 4, and 5 shown in Fig. 16. For the brine with a high Ca^{2+} ion concentration, with an increase in Mg^{2+} ion concentration, all $Mg(OH)_2$ crystals were agglomerated morphology, as pictures 7, 8, 9, and 10 shown in Fig. 16.

The changes in Ca^{2+} and Mg^{2+} ion concentration would affect the $CaCO_3$ crystal morphologies. When the Mg^{2+} ions were high, and with an increase in Ca^{2+} ion concentrations, the $CaCO_3$ content in the scaling increases. When a large number of polar $CaCO_3$ crystals were attached, the polar $Mg(OH)_2$ crystals would slip and form agglomerates through dislocations during the formation process under external polar force. The $CaCO_3$ crystal cracked and split into irregular crystals (higher Mg^{2+} ion concentrations). When the Ca^{2+} ions were high, the Mg^{2+} ion concentration also increased, which made it easier for Mg^{2+} ions to replace Ca^{2+} ions in the lattices, which made the $CaCO_3$ crystals easy to break and form amorphous crystals. In the presence of Mg^{2+} ions, the $Mg(OH)_2$ crystals presented a honeycomb agglomerated morphology (higher Ca^{2+} ion concentrations).

Higher Mg^{2+} ion concentrations would increase the ionic strength of the solution and increase $CaCO_3$ supersaturation [20], but the effects of Mg^{2+} ions on the solution's ionic strength decreased with an increase in Ca^{2+} ion concentration. Therefore, the strong effect of Mg^{2+} ions exceeded its inhibition on $CaCO_3$. Therefore, an appropriate Mg^{2+} ion concentration would be more beneficial to $CaCO_3$ crystals that split into scattered irregular crystals on the aluminum brass tube surface.

From the aforementioned experimental results, it could be seen that the $Mg(OH)_2$ crystals existed regardless of the Mg^{2+} ion concentration, except for the brine without Mg^{2+} ions at all. The crystal particle sizes for $CaCO_3$ were far larger than that of $Mg(OH)_2$, but scaling in the brine containing Ca^{2+} ions, the $CaCO_3$ crystal amount was generally larger than that of $Mg(OH)_2$.

4. Conclusions

The effects of Ca^{2+} and Mg^{2+} ion concentrations in brine on the formation and morphologies of scale were investigated and experimented on. The following were concluded:

- According to the proportion of main components in natural seawater, concentrated brine was prepared. Under a constant temperature of 80°C, scaling would occur on the metal surface, and the main components for scaling were $CaCO_3$ crystal and $Mg(OH)_2$ crystal.
- Under the condition that no Mg^{2+} ions were in the brine, and under the potential of NaCl, $CaCO_3$ crystal morphologies were primarily overlapped when they were plate-like, containing both hexahedral crystals and needle-like crystals. With an increase in the Mg^{2+} ion concentration, due to the polarity inherent in $Mg(OH)_2$ crystals, the $CaCO_3$ crystal morphology transformed into a regular octahedral crystal. Further increasing the Mg^{2+} ion concentration, the $CaCO_3$ crystals appeared cracked due to lattice distortion and split into irregular crystals.
- Under the condition that no Ca^{2+} ions were in the brine, the tube surface was evenly covered with a scale layer primarily composed of $Mg(OH)_2$ crystals. The $Mg(OH)_2$ crystals showed the morphology for the triangular cone. With an increase in Ca^{2+} ion concentration, due to the polarity of the $CaCO_3$ crystals, the $Mg(OH)_2$ crystal morphologies changed to flake and formed a honeycomb agglomeration, and the $CaCO_3$ crystal appeared cracked due to lattice distortion and split into irregular crystals (higher Mg^{2+} ion concentrations).
- Under experimental conditions, a higher Mg^{2+} ion concentration would increase the ionic strength of the solution and increase $CaCO_3$ supersaturation, but the effects of the Mg^{2+} ions on the ionic strength of the solution decreased with an increase in Ca^{2+} ion concentration. Therefore, an appropriate amount of Mg^{2+} ions could make $CaCO_3$ crystals split into scattered irregular crystals on the aluminum brass tube surface.
- The development of the $CaCO_3$ crystal was in the morphology of octahedron. The crystal size of $CaCO_3$ was much larger than that of $Mg(OH)_2$. Generally speaking, the amount of $CaCO_3$ crystals is larger than that of $Mg(OH)_2$ crystal.

Acknowledgments

The authors are grateful to the Key Projects of the Natural Science Foundation of China (51936002) and the Major Science and Technology Projects of Liaoning Province (2019JH1/10300003) for their financial support.

References

[1] S.M. Alsadaie, I.M. Mujtaba, Dynamic modelling of heat exchanger fouling in multistage flash (MSF) desalination, Desalination, 409 (2017) 47–65.
[2] T.M. Pääkkönen, M. Riihimäki, C.J. Simonson, Crystallization fouling of $CaCO_3$–analysis of experimental thermal resistance and its uncertainty, Int. J. Heat Mass Transfer, 55 (2012) 6927–6937.
[3] S.M. Peyghambarzadeh, N. Bahrami, Statistical analysis of calcium sulfate scaling under boiling heat transfer, Appl. Therm. Eng., 53 (2013) 108–113.
[4] H. Xu, H.S. Li, D. Wang, Study on $CaSO_4$ crystallization process and its influential factors, Ind. Water Treat., 31 (2011) 67–69.
[5] A.E. Al-Rawajfeh, Modeling of alkaline scale formation in falling film horizontal-tube multiple-effect distillers, Desalination, 205 (2007) 124–139.
[6] S.Y. Liu, Experimental Research of Seawater Fouling Process on Falling-Film Evaporation Outside Horizontal Tube, Dalian University of Technology, 2014.
[7] S.N. Kazi, G.G. Duffy, X.D. Chen, Fouling and fouling mitigation on heated metal surfaces, Desalination, 288 (2012) 126–134.
[8] H.U. Zettler, M. Wei, Q. Zhao, Influence of surface properties and characteristics on fouling in plate heat exchangers, Heat Transfer Eng., 26 (2005) 3–17.
[9] A. Stärk, K. Krömer, H. Glade, Impact of tube surface properties on crystallization fouling in falling film evaporators for seawater desalination, Heat Transfer Eng., 38 (2017) 207–217.
[10] C. Wildebrand, H. Glade, S. Will, Effects of process parameters and anti-scalants on scale formation in horizontal tube falling film evaporators, Desalination, 204 (2007) 448–463.
[11] K. Krömer, S. Will, K. Loisel, Scale formation and mitigation of mixed salts in horizontal tube falling film evaporators for seawater desalination, Heat Transfer Eng., 36 (2014) 750–762.

[12] A. Stärk, K. Loisel, K. Odiot, Wetting behaviour of different tube materials and its influence on scale formation in multiple-effect distillers, Desal. Water Treat., 55 (2015) 2502–2514.
[13] Z.X. Chen, L.P. Zhang, H. Ma, Effect of Na^+ for the in-suit growth of magnesium hydroxide crystals on the cellulose membrane and their applications, J. Donghua Univ., 39 (2013) 322–326.
[14] F. Al-Hazmi, A. Umar, G.N. Dar, Microwave assisted rapid growth of $Mg(OH)_2$ nanosheet networks for ethanol chemical sensor application, J. Alloys Compd., 519 (2012) 4–8.
[15] X. Song, S. Sun, D. Zhang, Synthesis and characterization of magnesium hydroxide by batch reaction crystallization, Front. Chem. Sci. Eng., 5 (2011) 416–421.
[16] D. Yi, G. Zhang, W. Hao, Nanoscale magnesium hydroxide and magnesium oxide powders: control over size, shape, and structure via hydrothermal synthesis, Chem. Mater., 13 (2001) 435–440.
[17] W. Zhen, J.H. Davidson, L.F. Francis, Effect of water chemistry on calcium carbonate deposition on metal and polymer surfaces, J. Colloid Interface Sci., 343 (2010) 176–187.
[18] Z.F. Liu, M.F. Yan, L.H. Zhang, Study on the effect of magnesium ion on the crystal of calcium carbonate, Technol. Water Treat., 37 (2011) 60–62.
[19] Z.Y. Zhang, R.A. Dawe, Influence of Mg^{2+} on the kinetics of calcite precipitation and calcite crystal morphology, Chem. Geol., 163 (2000) 129–138.
[20] C.F. Yang, D.Q. Xu, Z.Q. Shen, The effect of surface material and Mg^{2+} on the scaling of $CaCO_3$, J. Chem. Eng. Chin. Univ., 8 (1994) 313–317.
[21] B. Ni, S.Q. Shen, X.H. Liu, S. Chen, Effects of temperature and salinity on fouling in hypersaline seawater, Desal. Water Treat., 173 (2020) 41–48.
[22] J.Z. Chen, Modern Crystal Chemistry, Science Press, Beijing, 2010, pp. 65–93.
[23] Y. Takita, M. Eto, H. Sugihara, Promotion mechanism of co-existing NaCl in the synthesis of $CaCO_3$ Mater. Lett., 61 (2007) 3083–3085.